Article

Development of High-Sensitivity Thermoplastic Polyurethane/Single-Walled Carbon Nanotube Strain Sensors through Solution Electrospinning Process Technique

Athanasios Kotrotsos [1], Nikolaos Syrmpopoulos [1], Prokopios Gavathas [1], Sorina Moica [2] and Vassilis Kostopoulos [1,3,*]

[1] Department of Mechanical Engineering and Aeronautics, University of Patras, Patras University Campus, GR-26504 Patras, Greece; akotrotso@mech.upatras.gr (A.K.); nikos.syr@hotmail.com (N.S.); prokopisgabathas@gmail.com (P.G.)

[2] Department of Industrial Engineering and Management, The George Emil Palade University of Medicine, Pharmacy, Science and Technology of Targu Mures, 540142 Targu Mures, Romania; sorina.moica@umfst.ro

[3] Foundation of Research and Technology, Institute of Chemical Engineering Sciences (FORTH/ICE-HT), Studious Str., GR-26504 Patras, Greece

* Correspondence: kostopoulos@upatras.gr; Tel.: +30-2610-969441

Abstract: In this study, nanofibers obtained through the electrospinning process are explored for strain-sensing applications. Thermoplastic polyurethane (TPU) flexible structures were fabricated using the solution electrospinning process (SEP) technique. Subsequently, these structures were nanomodified with single-walled carbon nanotubes (SWCNTs) through immersion into an ultrasonicated suspension containing 0.3 wt% SWCNTs. The nanomodification aimed to impart an electrically conductive network to the structures. Micro-tensile tests and electrical resistance measurements were conducted to characterize the apparent mechanical and electrical properties, respectively. The fabricated structures demonstrated potential as wearable strain sensors for monitoring changes in strain across various applications. The samples exhibited excellent performance, high sensitivity, outstanding mechanical properties, and a broad stretching range. Scanning electron microscopy (SEM) observations provided qualitative insights into the activated conductive pathways during operation.

Keywords: solution electrospinning; thermoplastic polyurethane; single-walled carbon nanotubes; strain-sensing; tensile properties; flax/epoxy composites; structural health monitoring

1. Introduction

Responsive materials such as self-healing polymers, piezoelectric and hygromorphic materials, pH-sensitive hydrogels, electroactive polymers, etc., are a class of smart materials that exhibit controllable properties by the application of an external stimulus [1]. Based on the existing literature, the stimulus could be temperature [2], pressure [3], pH [4], moisture [5], light [6], chemical compounds [7], or force and extension [8]. These properties can be identified when these materials (i.e., sensors) are deposited onto conductive electrodes for the changes in electrical resistance to be measured. Indeed, traditional conductive materials like metals, semiconductors, and ceramics often struggle to meet the demands of modern applications requiring high sensitivity and stretchability. As a result, there is growing interest in developing innovative materials composed of flexible polymer matrices containing conductive nanofillers for strain-sensing applications. When integrated with electronics, these materials can function as sensors, offering improved sensitivity and stretchability compared to conventional materials [9,10]. This approach opens up new possibilities for creating advanced strain-sensing devices suitable for a wide range of applications.

One of the most popular ways to fabricate such structures is the electrospinning process (EP) technique [11]. A typical electrospinning instrument consists of three basic parts:

a power supply, a solution reservoir connected with a nozzle, and a collector. EP is an effective and low-cost method used to produce ultra-fine fibers or fibrous structures from polymers with a fiber diameter ranging from several micrometers to a few nanometers. By using the high-voltage electrostatic electric field, polymer solutions or melts are converted into polymeric fibers. The fabricated structures have a high surface-to-volume ratio, which makes them very attractive for a wide range of applications (i.e., sensors, biomaterials, nanocomposites, filters, etc.). Taking into consideration the solution electrospinning process (SEP), a wide range of natural and synthetic polymers or the blending of them have been successfully electrospun into fibrous structures [12–15]. Nano-filles have also been incorporated into polymeric fibers through the SEP, with the aim of enhancing the mechanical and/or electrical properties of them [9,13]. In addition, by using the EP, the structural characteristics of the fabricated structures can be controlled by the processing parameters (i.e., voltage, flow rate, distance, etc.) [16].

Polyurethanes (PUs) comprise a family of polymers which are characterized as versatile, with widely ranging properties and uses. PUs, when electrospun, present excellent stretchability, good porosity, and good mechanical properties that make them potential candidates for many applications [17]. The potential applications involve biomedicine (i.e., scaffolds for bone tissue engineering and for blood vessels), protective clothing, and wound dressing [18–21]. In [22], the authors combined a silica precursor (i.e., polyvinyltrimethoxysilane) together with electrospun TPU nanofibers in the aerogel backbone to create effective stress transfer pathways in three-dimensional aerogel composites with thermal insulation characteristics and a special porous structure. TPU composites containing gallium and indium were also fabricated by using the SEP method, with the aim of acting as potential material for shielding against medical diagnostic X-rays [23]. Another property of the electrospun PU is the shape memory capability [24]. Based on the existing literature, PUs, when dissolved into dimethylformamide (DMF) or tetrahydrofuran (THF)/DMF mixture and electrospun, provide ultrathin fibers and uniform fibrous structures that make it very attractive for strain-sensing applications [25,26].

In [8], Mojtaba et al. fabricated electrically conductive PU nanofibers by the modification of them with multi-walled carbon nanotubes (MWCNTs) through the SE process. By modification, it was shown that the fiber diameter and the mechanical properties were enhanced, while the reversibility of the electrical properties was studied by testing them under cycling loading conditions. In [27], Wang et al. also fabricated a flexible thermoplastic PU (TPU)/MWCNTs strain sensor by the SE process and dip-coating procedure. The sensors demonstrated high sensitivity and durability, along with favorable mechanical properties. Additionally, a novel empirical model was introduced to predict the conductive response during the stretching of the fabricated sensor. Apart from materials within the PU family, various elastomeric polymers have been employed as matrices for the fabrication of conductive sensors. Ecoflex [28], polydimethylsiloxane [29], nylon, and nitrile butadiene rubber [30] are potential candidates due to their high flexibility and reversible deformation characteristics. Apart from the thermoplastic type of strain sensors, thermoset ones also exist in the literature. Interestingly, in [31], CNT sheet layers were distributed through the thickness of a glass-fiber-reinforced plastic composite structure to act as a sensor after the polymerization of the thermoset matrix. The in-plane change in the electrical resistance value after an impact event was able to detect the presence of damage. Finally, in [32], the authors loaded an adhesive with CNTs to take advantage of their electrically conductive network. The conductive adhesive was utilized for structural health monitoring in adhesive joints.

In the present study, a high-performance TPU/SWCNT strain sensor was successfully fabricated using the SEP technique. Specifically, electrospun TPU structures were immersed in a suspension containing distilled water and SWCNTs at a concentration of 0.3 wt% for 2 h to establish conductive paths via the ultrasonication method. Following nanomodification, the samples were placed in a conventional oven to remove humidity. Micro-tensile tests were executed to unveil the apparent mechanical properties after the nanomodification

and drying process, while electrical resistance measurements were conducted concurrently. In addition, electrical resistance measurements were conducted in the through-the-thickness direction, while SEM observations led to qualitative insights regarding the fiber diameter, the porosity, as well as the SWCNT conductive network that was fabricated along the electrospun TPU structure. Finally, the fabricated TPU/SWCNT structures demonstrated potential as wearable strain sensors for monitoring strain across various applications.

2. Materials and Methods

2.1. Raw Materials

The TPU utilized as the matrix for the strain sensor, under the trade name "Elastolan 1180A", was provided by BASF Polyurethanes GmbH, Lemfoerde, Germany. The TPU material, received in pellet form, had a density of 1.11 g/cm^3. SWCNTs were employed as nanofillers, specifically the NTX9 type supplied by Nanocyl, Sambreville, Belgium, and produced via the Catalytic Chemical Vapor Deposition (CCVD) process. These SWCNTs typically exhibit diameters ranging between 0.8 and 1.4 nm and lengths equal to or greater than 5 µm.

For solvent usage, tetrahydrofuran (THF) and N, N dimethylformamide (DMF) were employed, both purchased from Sigma Aldrich, Saint Louis, USA, with a purity of ≥99%. In terms of applying the fabricated strain sensor to a composite structure during a tensile test, the fabricated composite was epoxy resin-based, reinforced by flax fibers. The epoxy system comprised epoxy resin L and hardener EPH 161, provided by R & G Faserver- bundwerkstoffe GmbH, Stuttgart, Germany, mixed in a stoichiometric ratio of 4:1 *w/w*.

The liquid-form epoxy resin L has a yellowish color and a density of 1.14 g/cm^3. The EPH 161 hardener features a processing time of 90 min when mixed with the epoxy resin L, and the curing temperature initiates from 18 °C. As for the flax fabric, the ampliTex Art. No. 5040 balanced weave (00/900) with an aerial weave weight of 300 gsm was utilized and supplied by Bcomp company, Fribourg, Switzerland. The precise flax fabric is known for its excellent drapability and suitability for forming complex shapes.

2.2. Solution Preparation and Solution Electrospinning Process (SEP)

To create TPU structures intended for use as strain sensors in various applications, we employed the SEP technique. TPU pellets, comprising 10 wt% of the solution, were dissolved in a solvent mixture of DMF/THF (stoichiometric ratio of 1:1). The mixture was then stirred magnetically overnight at room temperature (RT) conditions to achieve a uniform solution. Subsequently, the prepared TPU solution was transferred into a 10 mL syringe and directly electrospun onto a grounded aluminum-foil-covered collector measuring 15 × 15 cm^2. During the SEP, the solution flow rate was maintained at 0.2 mL/h, and a constant voltage of 20 kV was applied to ensure continuous jet formation. The distance between the nozzle tip and the collector was set at 13 cm, utilizing a metallic 25 gauge (G25) hypodermic needle with an inner diameter of 0.43 mm. The SEP was conducted under ambient conditions. A custom-made SEP setup was employed for the purposes of this study.

2.3. TPU/SWCNT Strain Sensor Fabrication

To fabricate the TPU strain sensor, the fibrous TPU structures produced through the SEP were immersed in a suspension containing ultrasonicated SWCNTs using the dip- coating method. Specifically, the suspension comprised distilled water and SWCNTs at a concentration of 0.3 wt%, taking into consideration reference [27]. Six strips, each measuring 60 × 30 × 0.2 mm^3, were immersed in the suspension for two hours. Before and after immersion, ultrasonication was used to disperse the SWCNTs and prevent aggregation. The utilized ultrasonic bath was the SONOREX (tradename) with a working frequency of 35 kHz and was supplied by Bandelin GmbH & Co. company, Berlin, Germany. Upon completion of the immersion and nanomodification process, the samples were removed from the suspension and washed twice with distilled water to eliminate any potentially

unanchored SWCNTs. Subsequently, they were dried in a conventional oven at 80 °C for 30 min. Following the nanomodification process, the final TPU strain sensor was estimated to contain SWCNTs at a concentration of 1.76 wt%. Six samples, each with dimensions of $30 \times 10 \times 0.2$ mm^3, were punched out to serve as strain sensors for further investigation.

2.4. Flax/Epoxy Composites Fabrication

For this study, a single type of laminated flax/epoxy composite plate was produced, consisting of 8 plies of woven (0°/90°) flax dry fabric. The manufacturing process involved laying up the plies, followed by vacuum bagging, infusion, and curing at ambient conditions for 24 h, adhering to the guidelines provided by the epoxy resin manufacturer. The final plates measured $270 \times 150 \times 4.5$ mm^3 in dimensions, with a calculated fiber volume fraction (V_f) estimated to be approximately $40 \pm 2\%$.

2.5. Scanning Electron Microscopy (SEM) and Microstructure Analysis

The morphology and microstructure of the fabricated layers were assessed using SEM. For SEM analysis, square strips measuring 5×5 mm^2 were machine- and sputter-coated with gold for 30 s. Subsequently, the samples were inserted into a field emission scanning electron microscopy instrument (FE-SEM, FEI InspectTM F50) equipped with a scanning electron detector. The FE-SEM operated at 5 kV and was supplied by FEI company, Hillsboro, OR, USA. To determine the fiber diameter measurements, SEM micrographs were processed using ImageJ software, Version win64 (NIH, Bethesda, MD, USA). By applying different thresholds, SEM images were converted to binary images. A minimum of 150 fiber diameters were measured, with 50 measurements taken from three different samples' images. The average value and standard deviation (SSD) were then reported. Furthermore, a statistical analysis of the measured fiber diameter values was conducted using OriginPro with a 95% confidence interval to determine the fiber diameter distribution that best describes the experimental data.

2.6. Uniaxial Tensile Tests and Electrical Resistance Measurements
2.6.1. TPU Samples

Five rectangular samples, each measuring 30 mm in length and 10 mm in width, were extracted from each electrospun layer. The thickness of each specimen was determined to be approximately 0.2 ± 0.01 mm using a thickness gauge. Constant force was applied during the measurements, and meticulous care was taken during sample preparation to prevent damage. Duct tape was delicately placed along the edges of the samples to enhance their mounting stiffness on the metallic grips of the testing device.

Uniaxial micro-tensile tests were conducted using a Minimat 2000 (Rheometric Scientific) tensile instrument equipped with a 200 N load cell. During the experiments, the span length was set at 10 mm. All tests were conducted RT until the sample failed at a strain rate of 2 mm/min. Prior to testing, pre-tension was applied to all samples to ensure extension and load receipt at the start of each experiment.

The apparent mechanical properties of the TPU structures, including apparent stress (σ) and strain (ε), can be calculated at any point during the tensile experiments using the following equations (Equations (1) and (2), respectively):

$$\sigma = \frac{F}{A} \tag{1}$$

$$\varepsilon = \frac{\Delta L}{L_o} \tag{2}$$

where F is the force, A is the cross-sectional area of the sample, ΔL is the displacement, and L_o is the initial span length. The apparent mechanical properties of the TPU electrospun structures, (i.e., the ultimate tensile strength (σ_{max}), Young's modulus (E), and the strain at break (ε_{max})) were measured and further analyzed.

During the tensile tests, electrical resistance measurements of the TPU strain sensors were recorded using a digital Keithley multimeter with an accuracy of 0.1 mΩ. To facilitate this, all the TPU samples were coated with silver paint at the ends of their top surfaces to create a conductive coating. This coating allowed for the positioning of the copper electrodes of the Keithley 2002 8.5 Digit Multimeter setup during the tensile tests.

Additionally, the metallic grips of the tensile machine were substituted with acrylonitrile butadiene styrene (ABS) 3D-printed grips to serve as insulators and ensure accurate measurements. Through-thickness electrical resistance measurements were also conducted using the same equipment.

2.6.2. Flax/Epoxy Composite Samples

The uniaxial tensile tests were carried out on balanced and symmetric flax/epoxy composite laminates, incorporating the TPU/SWCNTs strain sensor at the center of their span, following test method D 3039/D 3039M. Each sample measured $250 \times 25 \times 4.5$ mm^3, and the crosshead velocity was held constant at 2 mm/min. Testing was conducted using an Instron hydraulic machine (250 kN), with five samples subjected to analysis. The stress (σ) and strain (ε) were calculated using Equations (1) and (2), respectively, where ΔL represents displacement and Lo denotes the span length, which remained fixed at 150 mm throughout the experiments.

2.7. Porosimetry and Porosity

The average pore diameter of the fabricated samples was also determined by the image processing of SEM images with ImageJ software, Version win64 (NIH, Bethesda, MD, USA). The samples' porosity was determined from the ratio of the measured mass of the sample to the mass of a fully dense sample of the same size by measuring the sample's dimensions (i.e., length, width, and thickness). The thickness of all the samples was measured with a thickness gauge by applying constant force. The porosity was determined by using Equation (3) below:

$$P = \frac{M_1 - M_2}{M_1} \cdot 100 \; (\%) \tag{3}$$

where P is the porosity, M_1 is the mass of a fully compacted sample, and M_2 is the mass of an electrospun sample. All utilized samples had the same dimensions to ensure comparability.

3. Results

3.1. Test Outline Programme

Figure 1 provides a comprehensive visual representation of the experimental procedure conducted for the current investigation. The outlined steps include the following: (a) preparation of the TPU/DMF/THF solution with TPU material at 10 wt%, (b) implementation of the SEP technique to produce fibrous TPU structures, (c) nanomodification of the TPU structures through immersion in an ultrasonicated suspension containing SWCNTs at 0.3 wt%, followed by drying in a conventional oven at 80 °C for 30 min, (d) performance of micro-tensile tests combined with electrical resistance measurements, and, finally, (e) application of the fabricated strain sensor for (i) the detection of human motion and (ii) strain measurements during a uniaxial tensile test of a composite structure.

Furthermore, Figure 1 clearly distinguishes between the pure TPU electrospun mat, depicted in white, and the nanomodified mat resulting from immersion in the ultrasonicated SWCNT suspension, illustrated in black.
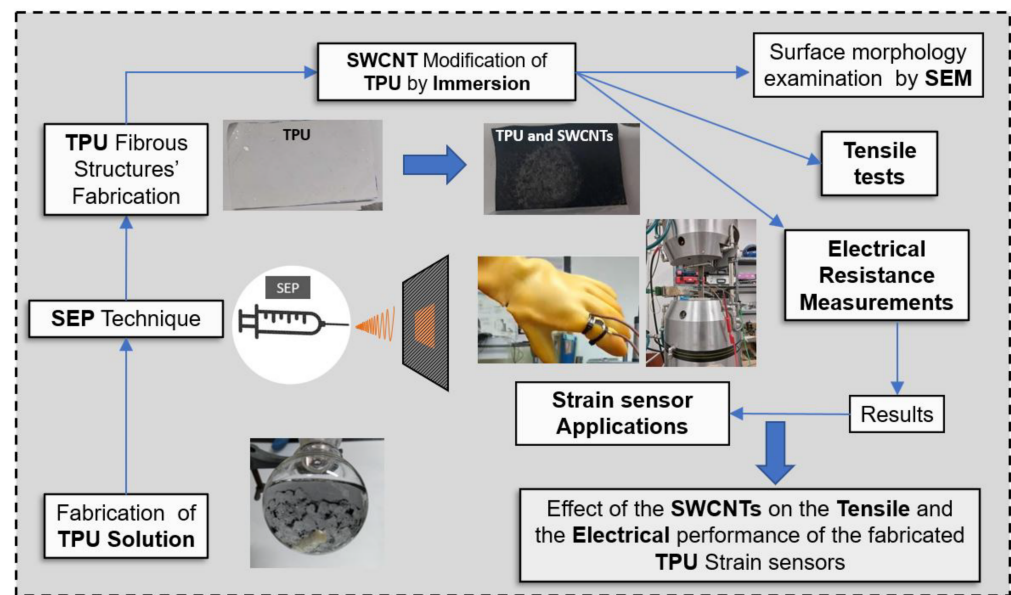
Figure 1. Illustration of the experimental campaign which was followed for the needs of the current investigation.

3.2. Uniaxial Tensile Properties and Electrical Resistance Measurements

For the fabrication of the final TPU/SWCNTs strain sensor, the initial electrospun TPU mats were immersed in a suspension of distilled water containing SWCNTs and then dried in an oven, as previously described. It is anticipated that the nanomodification procedure would impact the apparent mechanical properties of the final strain sensor. Uniaxial tensile tests were conducted according to the specifications outlined in Section 2.6.

In Figure 2A, representative stress (σ) vs. strain (ε, %) curves for both pristine TPU and the nanomodified TPU with SWCNTs (fabricated strain sensor) are depicted. For each structure, the apparent modulus of elasticity (E), maximum stress (σ_{max}), and maximum strain (ε_{max}, %) was calculated and presented in bar charts in Figure 2B–D. The general trend does not reveal any significant difference between the pristine TPU and SWCNT-modified structures. Initially, stress increases linearly, followed by a noticeable deviation from linearity. Subsequently, a plateau is formed, culminating in a load drop, leading to sample fracture.

The average modulus of elasticity (E) of pristine TPU structures was calculated to be 2.4 ± 0.6 MPa. Samples containing SWCNTs (1.76 wt%) exhibited an improved E value of 2.8 ± 0.6 MPa, representing a 14.5% increase. Similarly, σ_{max} values were enhanced by 72.5% (from 3.0 ± 0.6 MPa to 5.2 ± 0.8 MPa) after nanomodification. Moreover, ε_{max} (%) values were significantly improved by 81.5% (from $124.6 \pm 8.1\%$ to $225.2 \pm 20.7\%$) following nanomodification. Based on the experimental results, the presence of SWCNTs that led to reduced average pore diameter by 4.5% (5.33 ± 0.01 μm to 5.09 ± 0.01 μm) and porosity by 4.7% (from $28.55 \pm 0.10\%$ to $27.21 \pm 0.15\%$) enhanced the apparent mechanical properties of the fabricated strain sensor. The average pore diameter and porosity were calculated according to the specifications that are provided in Section 2.7. Toward this direction, the heating of the TPU sample after the immersion process (annealing) appears to also have a positive effect on the final apparent mechanical properties of the fabricated strain sensor. Similar behavior was observed in reference [33]. In addition, based on the literature, it was proved that the TPU itself creates a strong interfacial interaction with SWCNTs [34] and multi-walled CNTs [35], taking into consideration Fourier-transform infrared spectroscopy (FTIR) analysis. The main mechanism behind this behavior is the complete arrest of the inter- and intramolecular hydrogen bonding in the TPU/CNT system by CNTs that leads to improved mechanical performance.
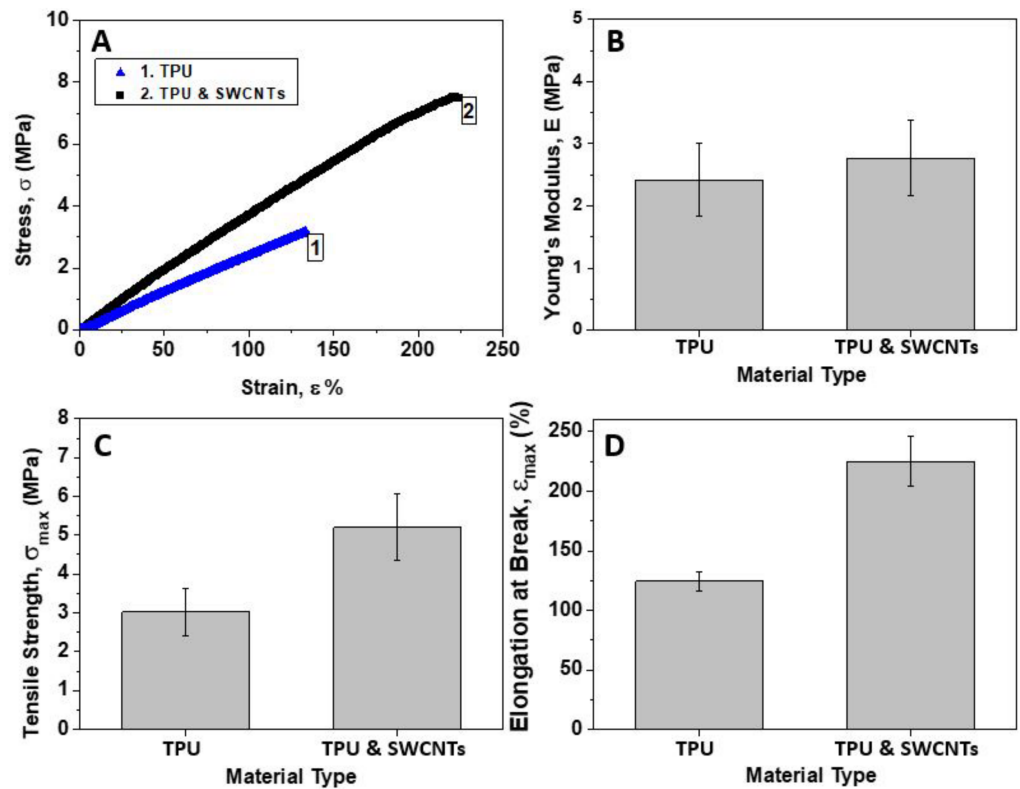
Figure 2. (**A**) Representative stress (σ) vs. strain (ε) % curves for pure TPU structure and the nano-modified one containing SWCNTs. Bar chart diagrams providing the tensile properties; (**B**) Young's modulus (E), (**C**) tensile strength (σ_max), and (**D**) elongation at break (ε_max). For all tensile properties, standard deviations (SSD) are provided.

Figure 3A provides a snapshot taken during the electromechanical tests conducted on the fabricated TPU/SWCNTs strain sensor. In this image, the electrodes for recording electrical resistance measurements and ABS grips are clearly visible. The ABS grips were manufactured and used to address isolation concerns between the sensor and the load applied set-up.

In our study, the TPU polymer in its electrospun form serves as the carrier for the conductive SWCNTs, allowing them to form a conductive network. According to the existing literature [8,27], the physical and mechanical properties of the TPU polymer facilitate the formation of ideal conductive paths by the conductive fillers, even under external stimulation. In our experimental set-up, the TPU/SWCNTs samples were tested using a combination of a tensile testing machine and a digital ammeter. The stretching rate during the micro-tensile tests was held constant at 2 mm/min, allowing us to record both the apparent mechanical properties and the electrical resistance simultaneously.

Figure 3B presents a schematic overview of the electromechanical performance of the fabricated strain sensor. In this analysis, we quantify the electromechanical response by considering the relative resistance variation in $\Delta R/R_0$ in relation to the tensile strain, ε (%). The equation for calculating the relative resistance variation is as follows:

$$\frac{\Delta R}{R_0} = \frac{R - R_0}{R_0} \tag{4}$$

where $\Delta R = R - R_0$, ΔR is the relative resistance variation; R and R_0 are the electrical resistance after and prior to deformation. It is evident that the relative resistance variation in $\Delta R/R_0$ consistently increases with the tensile strain, ε (%), until the point of fracture is reached. The operational range of a sensor is defined by the strain at which the actual

resistance exceeds the conductive range. Interestingly, in our study, the operational limit of the TPU/SWCNTs strain sensor was determined to be up to 220%.

When plotting the strain (ε) values against the corresponding $\Delta R/R_0$ values, the best-fitted curve was obtained using Equation (5). This equation will be further utilized to translate $\Delta R/R_0$ values into corresponding strain values for strain-sensing applications.

$$\varepsilon = -0.9610 * e^{-0.5127 * \frac{\Delta R}{R_0}} - 1.1981 * e^{-0.0499 * \frac{\Delta R}{R_0}} + 2.1829 e^{-0.0009 * \frac{\Delta R}{R_0}} \tag{5}$$
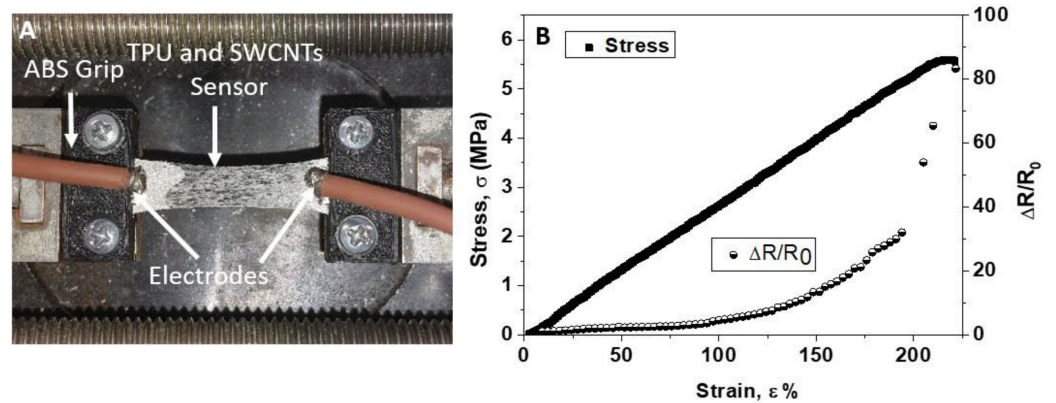
Figure 3. (**A**) Illustration of the fabricated TPU/SWCNTs strain sensor during a micro-tensile testing in which the electrodes and the 3D printing ABS grips are also clearly shown; (**B**) stress (σ) and $\Delta R/R_0$ versus strain; ε (%) curves of the fabricated TPU/SWCNTs strain sensor during the micro-tensile test.

The gauge factor (*GF*) is defined as the slope of the relative resistance variation in $\Delta R/R_0$ with respect to the strain curve, which reflects the sensitivity of the fabricated strain sensor. The equation for the *GF* calculation is as follows:

$$GF = \frac{d(\Delta R/R_0)}{d\varepsilon} \tag{6}$$

where ΔR represents the relative resistance variation, R_0 denotes the electrical resistance prior to deformation, and ε represents the strain experienced during tensile testing.

Figure 4 demonstrates that the gauge factor (GF) is not constant but rather monotonically increases with the strain, ε (%). Interestingly, the curve shows a significant increase in the GF value, exceeding 15 times from 100% strain (GF = 12) to 200% strain (GF = 187). Notably, for strains less than 50%, the GF factor remains nearly constant, calculated to be 3. This value is substantially higher than that of conventional strain gauges made from metallic wires, which typically have a GF close to 2 [36].
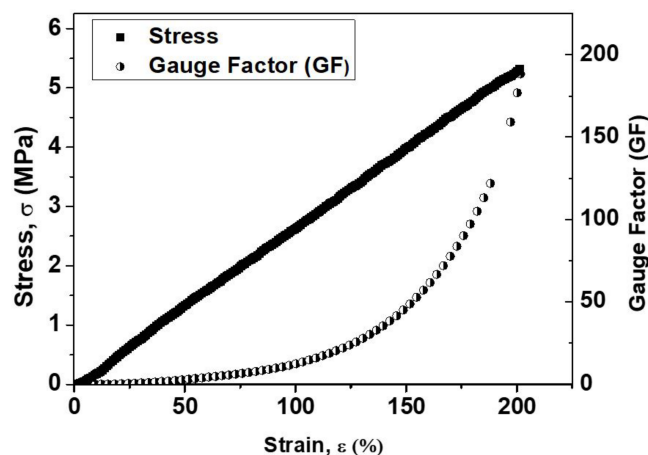

Figure 4. Gauge factor (GF) versus strain; ε (%) curve for the fabricated TPU/SWCNTs strain sensor.

The through-thickness measurements of the fabricated TPU/SWCNTs samples were also measured and further assessed. The four-probe method was utilized to measure the surface resistance of the fabricated strain sensor, employing the Keithley 2002 8.5 Digit Multimeter. The experimental set-up is clearly depicted in Figure 5A, where the fabricated strain sensor, with dimensions of $40 \times 40 \times 0.2$ mm^3, was positioned. Simultaneously, electrical resistance measurements were recorded under 2 and 3 bars of applied pressure.

Based on the experimental results, the sample exhibited conductivity, as evidenced by the calculated electrical resistance values of 33 ± 0.14 and 25 ± 0.15 Ohms, respectively. With an increase in applied pressure, the conductive networks become closer, resulting in a reduction in the electrical resistance value, thereby enhancing conductivity.
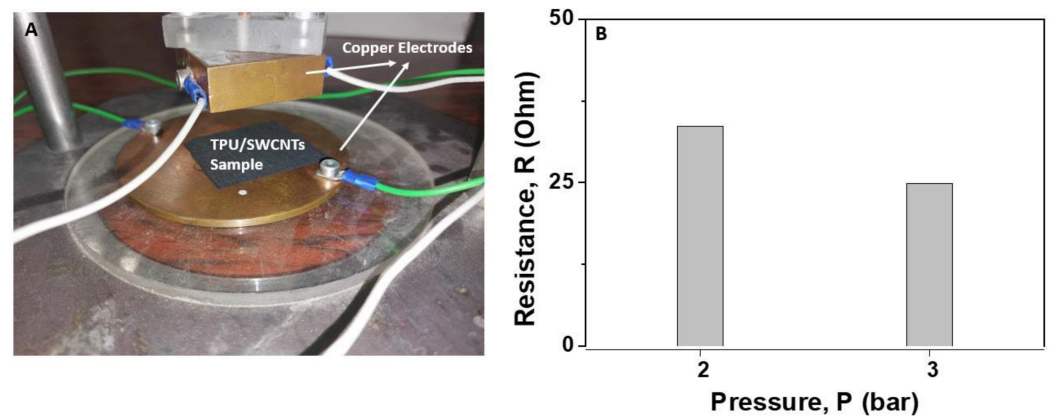
Figure 5. Through-the-thickness electrical resistance measurements. (**A**) Illustration of the utilized set-up; (**B**) bar chart diagram providing the through-the-thickness electrical resistance values by applying pressure to the TPU/SWCNTs mat of 2 and 3 bars, respectively.

3.3. Morphology Examination

In Figure 6, an SEM image showcases the fabricated TPU structure prior to the immersion and nanomodification process (Figure 6A), accompanied by a histogram depicting the distribution of the fiber diameters (Figure 6B). When examining Figure 6A, it becomes apparent that the structure consists of cylindrical, bead-free, non-woven fibers. These fibers exhibit smooth surfaces and form dense networks without any discernible alignment. The average fiber diameter, calculated from the histogram shown in Figure 6B, is determined to be 1.52 ± 0.7 μm.
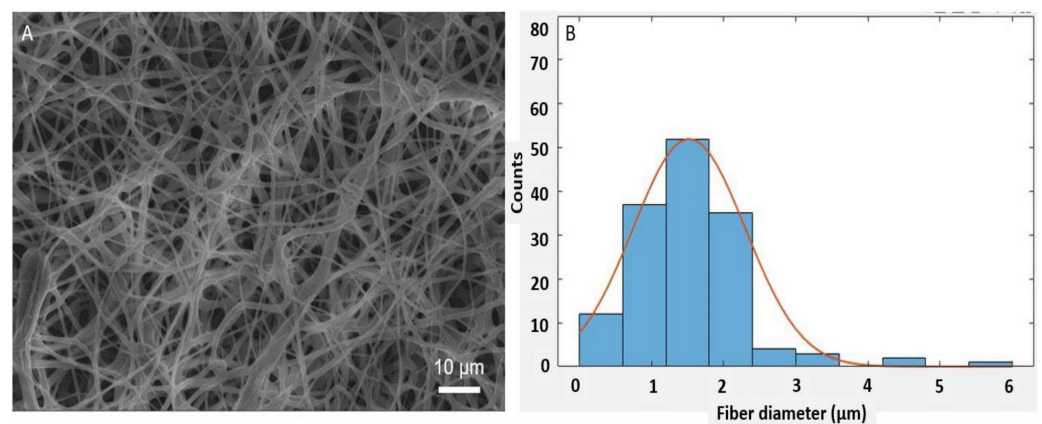

Figure 6. (**A**) Scanning electron microscopy (SEM) image of the initial electrospun TPU structure prior to immersion and (**B**) histogram providing the fiber diameter distribution for the fabricated electrospun TPU structure.

In Figure 7, the SEM image vividly displays the fabricated TPU/SWCNTs strain sensor. Upon closer examination of this image, it is evident that the SWCNTs have been successfully bonded to the electrospun TPU fibers following a two-hour immersion period in the suspension. Notably, the SWCNTs seem to be securely embedded within the electrospun TPU fiber structure, forming a stable and tight integration. Furthermore, due to dip-coating, the SWCNTs are also distributed within the pore areas between the TPU fibers. Overall, the SEM image reveals a uniform coverage of SWCNTs across the surface of the electrospun structure, facilitating the establishment of a conductive network.
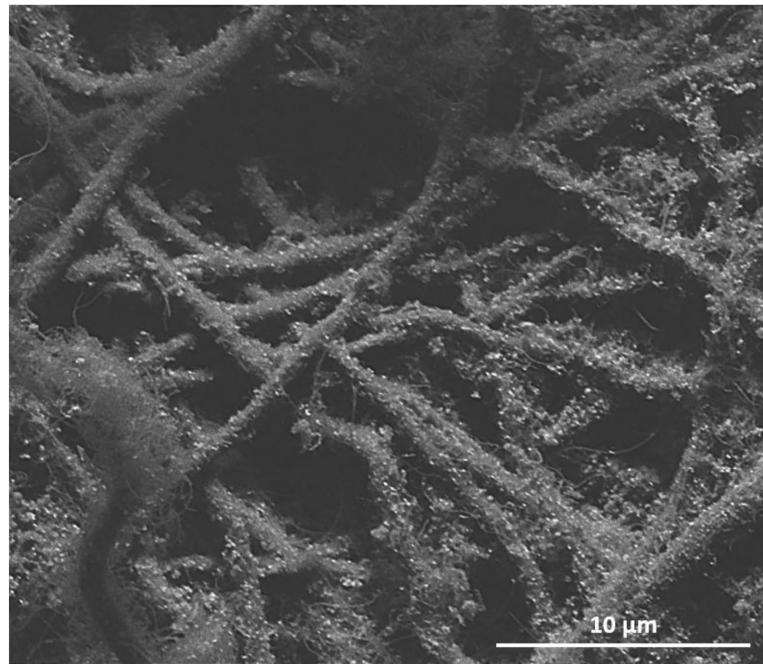
Figure 7. Scanning electron microscopy (SEM) image of the electrospun TPU structure after immersion procedure into suspension containing SWCNTs and drying.

3.4. Strain-Sensing Demonstration

3.4.1. Human Finger Motion Detection

Following the successful fabrication of the TPU/SWCNTs strain sensor, it was used to detect human finger motion, as clearly illustrated in Figure 8A. The figure also showcases the Keithley apparatus, responsible for measuring electrical resistance values during the movement. To facilitate finger motion detection, the strain sensor was securely positioned on the index finger using two clamps. These clamps served a dual purpose: not only did they ensure that the strain sensor remained in place during the demonstration, but they also accurately positioned the two electrodes for the precise recording of electrical resistance values. Additionally, to prevent electrical interference, an insulation glove was worn, which is particularly important as the strain sensor conducts electricity in the through-thickness direction (as outlined in Section 3.2). Figure 8B illustrates the recorded $\Delta R/R_0$ values of the fabricated TPU/SWCNTs strain sensor over time (t), while Figure 8C demonstrates how these values translate into strain (ε, %) using Equation (5).

The fluctuation observed in the $\Delta R/R_0$ value during the finger motion can be attributed to the elongation (increase) and relaxation (reduction) of the web. These movements cause specific resistance to increase and decrease in the existing continuous network by altering the gaps between the SWCNTs.
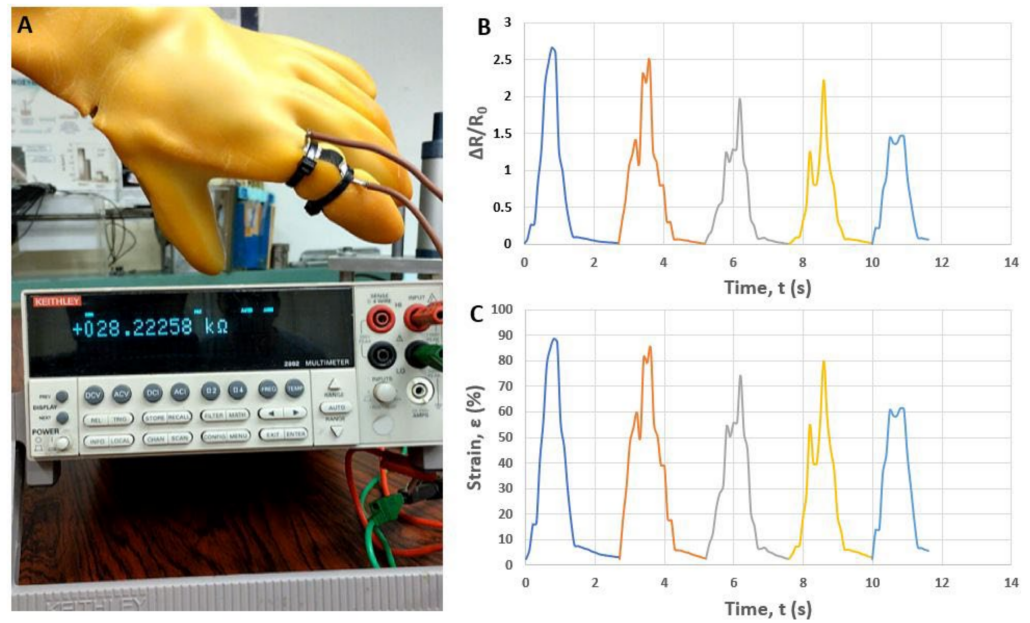
Figure 8. Sensing response of the TPU/SWCNTs strain sensor during a human motion. (**A**) Index finger bending and (**B**) $\Delta R/R_0$ versus time (t) and (**C**) translation of it into strain (ε, %) based on Equation (5).

3.4.2. Strain Recording during Tensile Experiments of a Flax/Epoxy Composites

Figure 9A depicts the fabricated TPU/SWCNTs strain sensor positioned at the gauge length of a flax/epoxy composite specimen, subjected to tensile loading. To ensure surface strain coupling, the strain sensor was glued on the surface of the test coupon. Subsequently, electrodes were positioned at both ends using silver paste and sturdy clips, as clearly shown in Figure 9A.
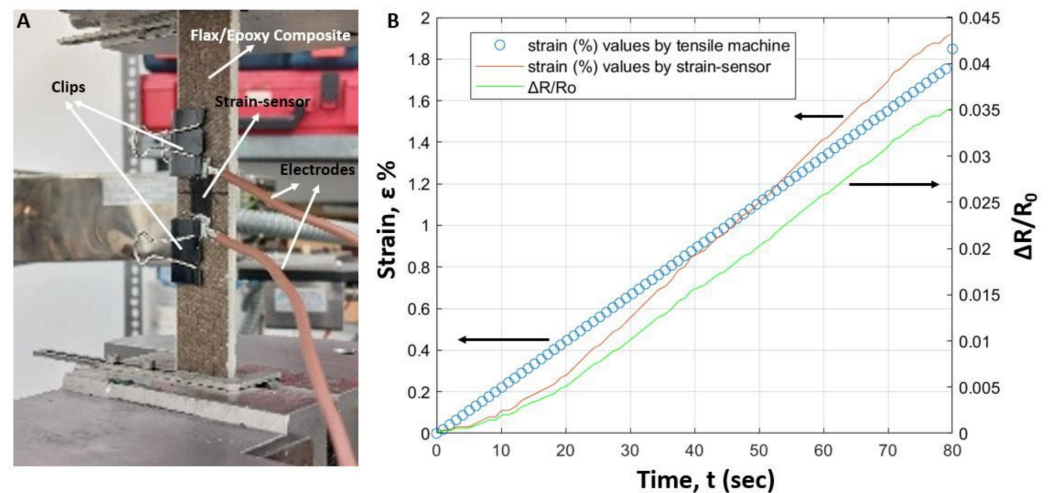
Figure 9. Sensing response of the TPU/SWCNTs strain sensor during a tensile test of a flax/epoxy composite structure. (**A**) Snapshot during a tensile test of the flax/epoxy specimen containing the fabricated TPU/SWCNTs strain sensor and (**B**) strain (ε, %) versus time (t) curve, that arose from the tensile instrument, $\Delta R/R_0$ versus time (t) curve, and translation of this curve into strain (ε, %) versus time (t), taking into consideration Equation (5).

During the tensile experiments, the flax/epoxy specimens were subjected to tension until fracture. The plots in Figure 9B illustrate the strain (ε, %) versus time (t), the variation in $\Delta R/R_0$, and the translated values of $\Delta R/R_0$ to strain (ε, %) during the tensile experiment. More precisely, the diagram consists of three curves: (i) strain (%) values obtained by the

clip gauge, (ii) $\Delta R/R_0$ values obtained from the fabricated strain sensor, and (iii) strain (ε, %) values derived from $\Delta R/R_0$ values using Equation (5), plotted against time. Considering the two strain (%) curves, it is evident that they exhibit very good agreement.

In Figure 10, stress (σ) versus strain (ε, %) curves of the flax/epoxy composite structure are presented, incorporating strain (ε, %) values obtained from two sources: curve 1 represents values derived from the tensile machine, while curve 2 represents values from the fabricated TPU strain sensor, calculated using Equation (5). As indicated in Figure 9A, the strain sensor was positioned at the center of the examined samples. The experimental results depicted in Figure 10 demonstrate that the obtained σ-ε (%) curves exhibit very good agreement between the two sources of the strain measurement. Utilizing these curves, the mechanical properties of the flax/epoxy composite under tensile loading were calculated. For both curves, Young's modulus was determined to be 8.5 ± 0.3 GPa, while the strength was calculated to be 117.4 ± 5.7 MPa.
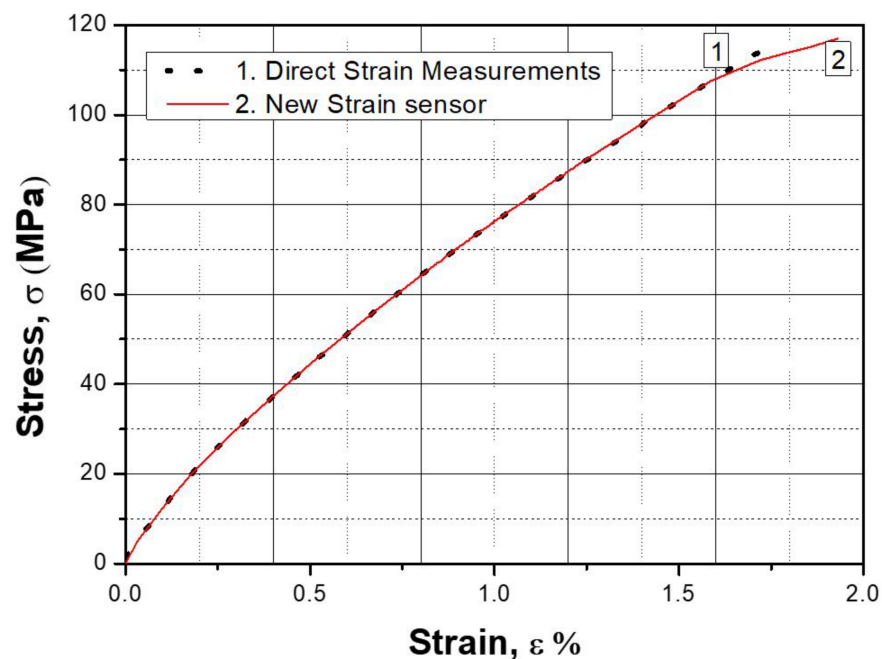

Figure 10. Stress (σ) versus strain (ε, %) curves of the flax/epoxy composite structure arose from the tensile tests which were conducted by taking into consideration the strain values obtained by the tensile machine (curve 1) and by the fabricated strain sensor (curve 2).

4. Conclusions

In this work, an electrically conductive nanostructure comprising the TPU polymer and SWCNTs has been successfully fabricated with the aim of acting as the strain sensor. For the fabrication of the strain sensor, the SEP technique was utilized to fabricate the TPU fibrous structure, while the dip-coating treatment was utilized to further nano-modify the electrospun structure and to endow it with an electrically conductive network. The apparent mechanical properties of the fabricated strain sensor were significantly increased after nanomodification due to the SWCNTs presence as well as due to the heating effect. Based on the experimental results, the fabricated strain sensor satisfied the fundamental requirements and is characterized by high sensitivity, flexibility, stretchability (strain > 200%), a wide working range of 0–200%, and repeatability. SEM images revealed the extended conductive network that has been fabricated as the SWCNTs were stably and tightly embedded into the electrospun TPU structure. In addition, electrical resistance measurements in the through-the-thickness direction revealed that the fabricated conductive network also works in the through-the-thickness direction. Furthermore, the applicability of the fabricated strain sensor as wearable sensing devices for human motion monitoring (i.e., as an electronic

skin) and as a strain gauge for strain monitoring during the tensile testing of composite structures has been successfully demonstrated.

References

1. Bai, W.; Jiang, Z.; Ribbe, A.E.; Thayumanavan, S. Smart organic two-dimensional materials based on a rational combination of non-covalent interactions. *Angew. Chem. Int. Ed.* **2016**, *55*, 10707–10711. [CrossRef] [PubMed]
2. Kotrotsos, A.; Kostopoulos, V. Self-healing of structural composites containing common thermoplastics enabled or not by-nanotechnology as healing agent. In *Book Self-Healing Composite Materials*, 1st ed.; Khan, A., Jawaid, M., Raveendran, S.N., Asiri, A.M.A., Eds.; Woodheal Publishing: Sawston, UK, 2020; Volume 18, pp. 327–374.
3. Shen, H.; Li, L.; Xu, D. Preparation of one-dimensional SnO_2-In_2O_3 nano-heterostructures and their gas-sensing property. *RSC Adv.* **2017**, *7*, 33098–33105. [CrossRef]
4. Pyo, J.Y.; Cho, W.J. In-plane-gate a-IGZO thin-film transistor for high sensitivity pH sensor applications. *Sens. Actuat. B-Chem.* **2018**, *276*, 101–106. [CrossRef]
5. You, M.H.; Yan, X.; Zhang, J.; Wang, X.X.; He, X.X.; Yu, M.; Ning, X.; Long, Y.Z. Colorimetric humidity sensors based on electrospun polyamide/$CoCl_2$ nanofibrous membranes. *Nanoscale Res. Lett.* **2017**, *12*, 360. [CrossRef] [PubMed]
6. Chen, S.; Long, Y.Z.; Zhang, H.D.; Liu, S.L.; Liu, L.Z.; Zhang, J.C.; Liu, G.X.; Shan, F.K. Fabrication of ultrathin In_2O_3 hollow fibers for UV light sensing. *Phys. Scr.* **2014**, *89*, 115808. [CrossRef]
7. Zhang, J.; Li, S.; Ju, D.D.; Li, X.; Zhang, J.C.; Yan, X.; Long, Y.Z.; Song, F. Flexible inorganic core-shell nanofibers endowed with tunable multicolor upconversion fluorescence for simultaneous monitoring dual drug delivery. *Chem. Eng. J.* **2018**, *349*, 554–561. [CrossRef]
8. Darbandi, S.M.A.; Nouri, M.; Mokhtari, J. Electrospun nanostructures based on polyurethane/MWCNTs for strain sensing applications. *Fibers Polym.* **2012**, *13*, 1126–1131. [CrossRef]
9. Hia, I.L.; Snyder, A.D.; Turicek, J.S.; Blanc, F.; Patrick, J.F.; Therriault, D. Electrically conductive and 3D-printable copolymer/MWCNT nanocomposites for strain sensing. *Compos. Sci. Technol.* **2022**, *232*, 109850. [CrossRef]
10. Haggenmueller, R.; Guthy, C.; Lukes, J.R.; Fischer, J.E.; Winey, K.I. Single wall carbon nanotube/polyethylene nanocomposites: Thermal and electrical conductivity. *Macromolecules* **2007**, *40*, 2417–2421. [CrossRef]
11. Doshi, J.; Reneker, D. Electrospinning process and applications of electrospun fibers. *J. Electrost.* **1995**, *35*, 151–160. [CrossRef]
12. Kostopoulos, V.; Kotrotsos, A.; Fouriki, K. Graphene Nanoplatelet-and Hydroxyapatite-Doped Supramolecular Electrospun Fibers as Potential Materials for Tissue Engineering and Cell Culture. *Int. J. Mol. Sci.* **2019**, *20*, 1674. [CrossRef] [PubMed]
13. Kostopoulos, V.; Kotrotsos, A.; Fouriki, K.; Kalarakis, A.; Portan, D. Fabrication and Characterization of Polyetherimide Electrospun Scaffolds Modified with Graphene Nano-Platelets and Hydroxyapatite Nano-Particles. *Int. J. Mol. Sci.* **2020**, *21*, 583. [CrossRef] [PubMed]
14. Repanas, A.; Kotrotsos, A.; Kostopoulos, V.; Glasmacher, B. MWCNT-doped Nylon electrospun fibers as materials for increasing damage tolerance of CFRPs in structural applications. *Int. J. Innov. Sci. Eng. Technol.* **2016**, *3*, 272–400.
15. Lobo, A.O.; Afewerki, S.; Machado de Paula, M.M.; Ghannadian, P.; Marciano, F.R.; Zhang, Y.S.; Webster, T.J.; Khademhosseini, A. Electrospun nanofiber blend with improved mechanical and biological performance. *Int. J. Nanomed.* **2018**, *13*, 7891–7903. [CrossRef] [PubMed]
16. Frenot, A.; Chronakis, I.S. Polymer nanofibers assembled by electrospinning. *Curr. Opin. Colloid Interface Sci.* **2003**, *8*, 64–75. [CrossRef]
17. Demir, M.M.; Yilgor, E.; Erman, B. Electrospun of polyurethane fibers. *Polymer* **2022**, *43*, 3303–3309. [CrossRef]
18. Wang, H.; Feng, Y.; Behl, M.; Lendlein, A.; Zhao, H.; Xiao, R.; Lu, J.; Zhang, L.; Guo, J. Hemocompatible polyurethane/gelatin-heparin nanofibrous scaffolds formed by a bi-layer electrospinning technique as potential artificial blood vessels Front. *Chem. Sci. Eng.* **2011**, *5*, 392–400.

19. Kim, S.E.; Heo, D.N.; Lee, J.B.; Kim, J.R.; Park, S.H.; Jeon, S.H.; Kwon, I.K. Electrospun gelatin/polyurethane blended nanofibers for wound healing. *Biomed. Mater.* **2009**, *4*, 044106. [CrossRef] [PubMed]

20. Gorji, M.; Jeddi, A.A.A.; Gharehaghaji, A.A. A review on emerging developments in thermal and moisture management by membrane-based clothing systems towards personal comfort. *J. Appl. Polym. Sci.* **2022**, *139*, e52416. [CrossRef]

21. Mistrya, P.; Chhabraa, R.; Mukea, S.; Narvekara, A.; Sathayea, S.; Jainb, R.; Dandekar, P. Fabrication and characterization of starch-TPU based nanofibers for wound healing applications. *Meter. Sci. Eng.* **2021**, *119*, 111316. [CrossRef] [PubMed]

22. Karamikamkar, S.; Abidli, A.; Tafreshi, O.A.; Ghaffari-Mosanenzadeh, S.; Buahom, P.; Naguib, H.E.; Park, C.B. Nanocomposite Aerogel Network Featuring High Surface Area and Superinsulation Properties. *Chem. Mater.* **2024**, *36*, 642–656. [CrossRef]

23. Wang, J.; Wang, K.; Wu, J.; Hu, J.; Mou, J.; Li, L.; Feng, Y.; Deng, Z. Preparation of eGaIn NDs/TPU Composites for X-ray Radiation Shielding Based on Electrostatic Spinning Technology. *Materials* **2024**, *17*, 272. [CrossRef] [PubMed]

24. Sáenz-Pérez, M.; Bashir, T.; Laza, J.M.; García-Barrasa, J.; Vilas, J.L.; Skrifvars, M.; León, L.M. Novel shape-memory polyurethane fibers for textile applications. *Tex. Res. J.* **2019**, *89*, 1027–1037. [CrossRef]

25. Lakshman, L.R.; Shalumon, K.T.; Nair, S.V.; Jayakumar, R.; Nair, S.V.J. Preparation of Silver Nanoparticles Incorporated Electrospun Polyurethane Nano-fibrous Mat for Wound Dressing. *Macromol. Sci. Part A Pure Appl. Chem.* **2010**, *47*, 1012–1018. [CrossRef]

26. Gorji, M.; Jeddi, A.A.A.; Gharehaghaji, A.A.J. Fabrication and characterization of polyurethane electrospun nanofiber membranes for protective clothing applications. *Appl. Polym. Sci.* **2012**, *125*, 4135–4141. [CrossRef]

27. Wang, X.; Qu, M.; Wu, K.; Schubert, D.W.; Liu, X. High sensitive thermoplastic polyurethane/carbon nanotubes flexible strain sensor fitting via novel optimization empirical model. *Adv. Compos. Hybrid Mater.* **2023**, *6*, 63. [CrossRef]

28. Xu, M.X.; Qi, J.J.; Feng, L.F.; Zhang, Y. Highly stretchable strain sensors with reduced graphene oxide sensing liquids for wearable electronics. *Nanoscale* **2018**, *10*, 5264–5271. [CrossRef] [PubMed]

29. Yu, Y.; Luo, Y.F.; Guo, A.; Yan, L.J.; Wu, Y.; Jiang, K.L.; Li, Q.Q.; Fan, S.S.; Wang, J.P. Flexible and transparent strain sensors based on super-aligned carbon nanotube films. *Nanoscale* **2017**, *9*, 6716–6723. [CrossRef] [PubMed]

30. Qu, M.C.; Qin, Y.J.; Sun, Y.; Xu, H.G.; Schubert, D.W.; Zheng, K.; Xu, W.; Nilsson, F. Biocompatible, flexible strain sensor fabricated with polydopamine-coated nanocomposites of nitrile rubber and carbon black. *ACS Appl. Mater. Interfaces.* **2020**, *12*, 42140–42152. [CrossRef] [PubMed]

31. Aly, K.; Bradford, P.D. Real-time impact damage sensing and localization in composites through embedded aligned carbon nanotube sheets. *Compos. B Eng.* **2019**, *162*, 522–531. [CrossRef]

32. Stetco, C.; Sam-Daliri, O.; Faller, L.M.; Zangl, H. Piezocapacitive sensing for structural health monitoring in adhesive joints. In Proceedings of the International Instrumentation and Measurement Technology Conference, Massey University, Auckland, New Zealand, 20–23 May 2019.

33. Sanchaniya, J.V.; Lasenko, I.; Kanukuntala, S.P.; Smogor, H.; Viluma-Gudmona, A.; Krasnikovs, A.; Tipans, I.; Gobins, V. Mechanical and Thermal Characterization of Annealed Oriented PAN Nanofibers. *Polymers* **2023**, *15*, 3287. [CrossRef] [PubMed]

34. Sankar, R.M.; Meera, K.S.; Mandal, A.B.; Jaisankar, S.N. Thermoplastic polyurethane/single-walled carbon nanotube composites with low electrical resistance. *High Perform. Polym.* **2013**, *25*, 135–146. [CrossRef]

35. Wang, X.; Xue, R.; Li, M.; Guo, X.; Liu, B.; Xu, W.; Wang, Z.; Liu, Y.; Wang, G. Strain and stress sensing properties of the MWCNT/TPU nanofiber film. *Surf. Interfaces* **2022**, *32*, 102132. [CrossRef]

36. Farcau, C.; Sangeetha, N.M.; Moreira, H.; Viallet, B.; Grisolia, J.; Ciuculescu-Pradines, D.; Ressier, L. High-Sensitivity Strain Gauge Based on a Single Wire of Gold Nanoparticles Fabricated by Stop-and-Go Convective Self-Assembly. *ACS Nano* **2011**, *5*, 7137–7143. [CrossRef] [PubMed]